BILINGUAL PUBLISHING GROUP

Journal of Environmental & Earth Sciences

https://journals.bilpubgroup.com/index.php/jees

ARTICLE

Magnetic Structure of Agadem Petroleum Block (Termit Basin, Eastern Niger): Analysis and Interpretation of Aeromagnetic Data

Abdourhamane Halidou Amadou

Intelligent Systems Georesources and Renewable Energy Laboratory, Faculty of Science and Technology, Sidi Mohamed Ben Abdallah University, Imouzzer Road, Fez BP: 2202, Morocco

ABSTRACT

The Agadem block is an area of major oil interest located in the large sedimentary basin of Termit, in the south-east of the Republic of Niger. Since the 1950s, this basin has known geological and geophysical research activities. However, despite the extensive research carried out, we believe that a geophysical contribution in terms of magnetic properties and their repercussions on the structure of the Agadem block allowing the improvement of existing knowledge is essential. The present study aims to study the structural characteristics of the Agadem block associated with magnetic anomalies. For this, after data shaping, several filtering techniques were applied to the aeromagnetic data to identify and map deep geological structures. The reduction to the pole map shows large negative wavelength anomalies in the southeast half of the block and short positive wavelength anomalies in the northwest part embedded in a large positive anomaly occupying the lower northern half of the block. The maps of the total horizontal derivative and tilt angle show lineaments globally distributed along the NW-SE direction in accordance with the structural style of the study area. The resulting map highlights numerous lineaments that may be associated with faults hidden by the sedimentary cover. The calculation of the Euler deconvolution allowed us to locate and estimate the depths of magnetic sources at variable depths of up to 4000 m. The compilation of the results obtained allowed us to locate zones of high and low intensities which correspond respectively to horsts and grabens as major structures of the Agadem block.

Keywords: Magnetic Structure; Reduction to the Pole; Magnetic Lineaments; Filtering; Interpretation; Agadem Block

*CORRESPONDING AUTHOR:

Abdourhamane Halidou Amadou, Intelligent Systems Georesources and Renewable Energy Laboratory, Faculty of Science and Technology, Sidi Mohamed Ben Abdallah University, Imouzzer Road, Fez BP: 2202, Morocco; Email: abdourhamane.halidou@usmba.ac.ma

ARTICLE INFO

Received: 19 August 2024 | Revised: 25 October 2024 | Accepted: 30 October 2024 | Published Online: 15 May 2025

DOI: https://doi.org/10.30564/jees.v7i5.7086

CITATION

Amadou, A.H., 2025. Magnetic Structure of Agadem Petroleum Block (Termit Basin, Eastern Niger): Analysis and Interpretation of Aeromagnetic Data. Journal of Environmental & Earth Sciences. 7(5): 492–506. DOI: https://doi.org/10.30564/jees.v7i5.7086

1. Introduction

Airborne geophysics is a method to geolocate and image homogeneously and continuously the surface and subsurface geological environment over very large areas in a short time [1]. Among its methods, the magnetic method occupies an important place in the exploration of mining and oil resources. Many geophysicists have successfully processed magnetic data to determine the magnetic properties and geometry of underground causal sources [2].

The purpose of the aeromagnetic method is to measure variations in the Earth's magnetic field caused by changes in the magnetic properties of geological structures and formations [3]. It is a method that can help to locate and delineate magnetic signatures and identify anomalous contacts and their depths [4].

In Niger, since the 1950s, the Termit sedimentary basin has been the subject of several geological and geophysical studies aiming to improve knowledge of its structure and oil potential. These studies have shown that this gigantic sedimentary basin, more than 600 km long and about 200 km wide, is structurally affected by polyphase play accidents [5]. Thus, two major phases of rifting are highlighted : The first dates from the Lower Cretaceous and is characterized by large NW-SE oriented fault blocks and the second from the Upper Senonian Paleogene represented by normal faults oriented NNW-SSE [6]. These extension phases are at the origin of the dislocation of the Termit basin, forming several sub-basins within the latter, including the Agadem sub-basin, also called the Agadem block. However, despite geological and geophysical works undertaken, we note a lack of detailed studies on magnetic anomalies that characterize the Agadem block.

In order to improve the existing knowledge of deep geological structures of the Agadem block, we consider that a detailed study, based on the interpretation of aeromagnetic data, is necessary. However it is important to stress that magnetic anomalies, once carefully processed, will highlight magnetic sources, in particular the volcanic lava, of which some evidence has been found to the east of the block, but also, and particularly, the topography of the substratum, in our case with an obvious magnetisation contrast with the sedimentary cover. To arrive at our results, sevral filters such as the reduction to the pole (RTP), the total horizontal derivative (THDR), the tilt angle (TA) and the 3D Euler deconvolution calculation were applied to the aeromagnetic data to facilitate their interpretation. This filtering process allowed to achieve the following results: the residual magnetic field map is established as well as the RTP map; magnetic anomalies of the study area are analyzed and characterized; magnetic lineaments are identified and digitalized from the THDR and TA maps. Finally, magnetic source depths are estimated and located.

2. Geographical Location of the Study Area

The Agadem block is located in the eastern of the Republic of Niger, about 1400 km from the capital Niamey. It covers most of the Termit sedimentary basin with an area of approximately 27000 km², is 300 km long from north to south and 60 to 110 km wide from east to west. The Agadem block is marked by coordinates 14°00' – 17°00' N and 12°00' – 14°00' E as indicated in **Figure 1**. Topographically, the Agadem block lies at the southern edge of the Sahara desert at an altitude of between 270 m and 470 m above sea level, with a generally high relief to the NW and a depression to the SE (**Figure 2**). The variable topography is mainly due to the formation of sand dunes in the form of waves. Despite the dry climate and the scarcity of vegetation, the area is rich in groundwater with aquifers lying less than 100 m deep.

3. Geological Setting

The Termit Basin is an intracontinental basin of Meso-Cenozoic age and is part of the West and Central African Rift System termed WCARS [6]. This rift system makes up a geotectonic continuum that extends 4000 km (**Figure 3**) from the Gao basin in Mali to the Anza basin in Kenya [7]. It is subdivided into two coeval Cretaceous genetically related but physically separated: the West African Rift Subsystem (WARS) which includes Mali, Niger and Nigeria and the Central African Rift Subsystem (CARS) composed of Chad, Cameroon, Kenya, and Re-

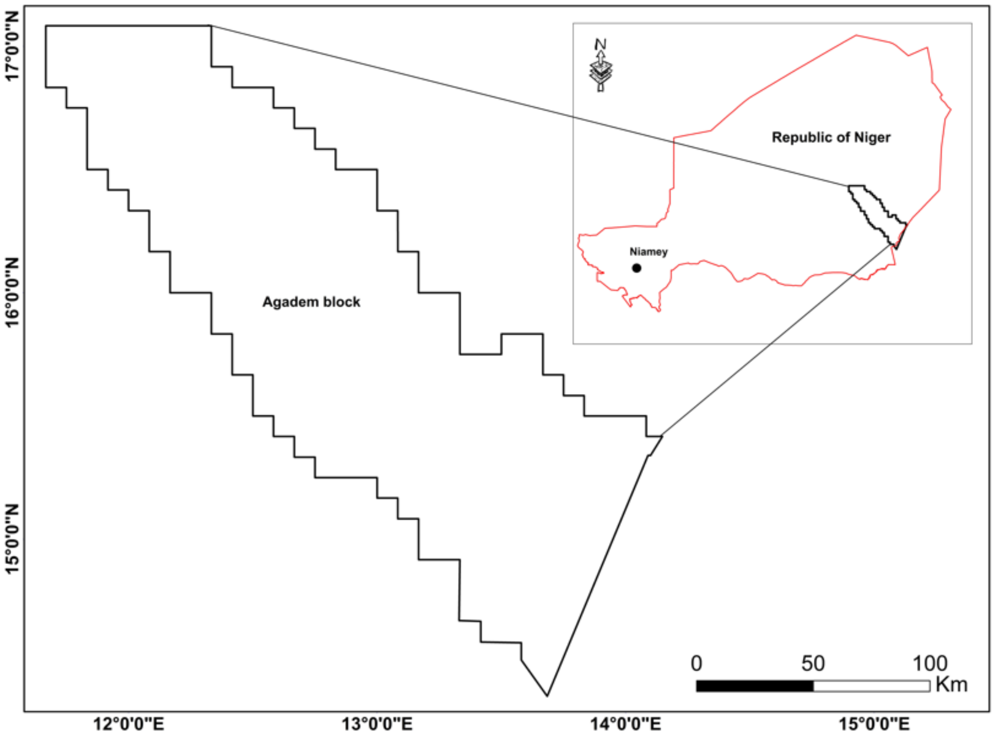

Figure 1. Geographical location of the Agadem block [7].

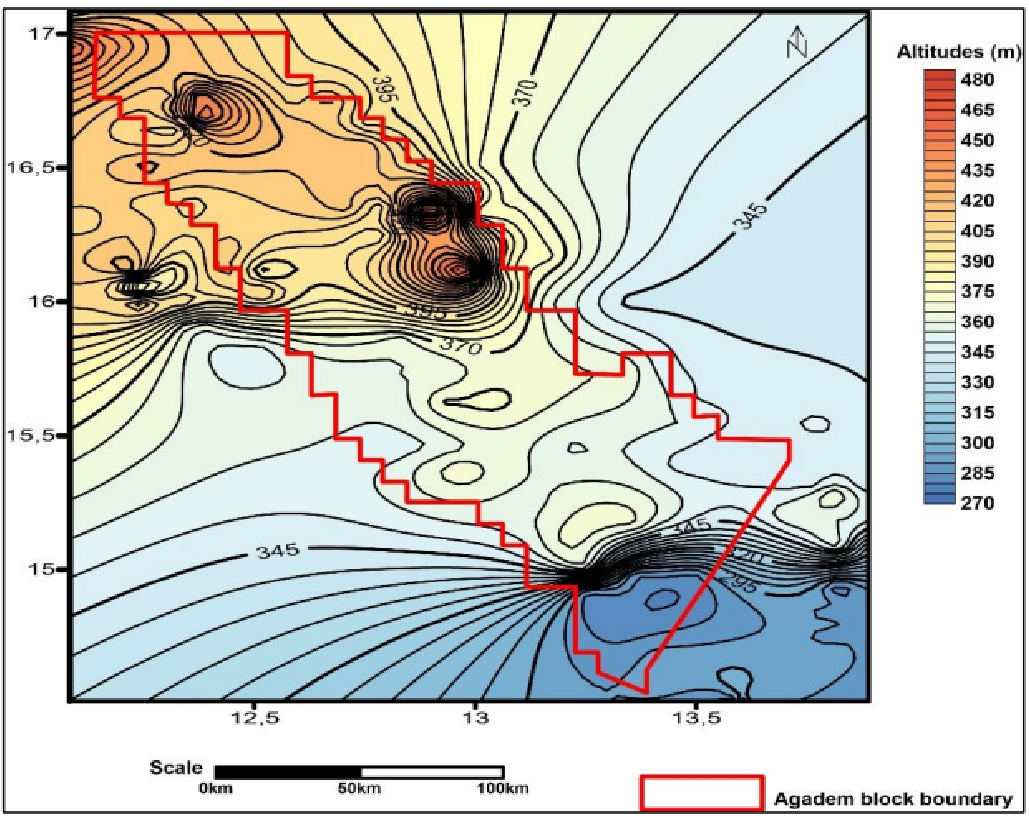

Figure 2. Topographical map of the Agadem block [7].

public of Central Africa and Sudan [6, 7].

The Termit Basin developed under the background of the opening of the South Atlantic in the Cretaceous. From the Early Aptian to Late Albian, the African-Arabian Plate extended in an NE-SW direction and pre-Pan-African metamorphic zones and Pan-African fold belts moved in NW-SE direction [8]. Intracontinental rift basins in East Niger, Chad, Sudan, etc. entered their initial syn-rift period and subsided rapidly along NW-SE boundary faults, giving rise to terrestrial sandstone and mudstone of thousands of meters [9]. In Late Cretaceous, syn-rift activities became weakened inside the African-Arabian Plate, when the global sea level reached its high in the Phanerozoic Eon and sea water came from Neo-Tethys Ocean and South Atlantic Ocean to bring on transgression on a large scale [9]. There was a trans-Saharan Seaway inside the African Plate, which separated the Hoggar uplift and Tibesti uplift and traversed Benue Trough, Chad, Algeria and Mali from the south to the north [8, 9]. At the end of the Cretaceous, the sea level descended and sediments in Central and West African basins were mainly of fluvial facies [10]. From the end of the Maastrichtian to the Early Paleocene, the African-Arabian Plate underwent regional uplift and was exposed to certain denudation in Upper Cretaceous [10]. In Paleocene and Middle Eocene, rifting activities occurred again in basins in Eastern Niger, Sudan, Kenya, etc. In Late Eocene (37 Ma), the African-Arabian Plate collided with the Eurasian Plate with tectonic compression in NNW-SSE inside the plate; after that, the African-Arabian Plate entered a period with active magmatic activities and active extension mainly in NEE-SWW or near E-W direction [10, 11]. Rift basins in the NW-SE direction in Central and West Africa entered intense syn-rifting stage and severe magmatic activities appeared at such weak crustal structures as Pan-African fold belts; for example, tholeiite eruption occurred on a large scale in the Hoggar district in north Termit Basin, which, together with faulted depression activities at the end of Eocene beginning of Oligocene, may all be responses in a same regional extensional setting [9]. At the beginning of the Miocene (~22 Ma), the African-Arabian Plate collided with the Eurasian Plate more violently and the internal plate was structurally compressed, uplifted and denuded [8]. From the Late Eocene to now, the Arabian Plate broke away from the African Plate and a rift system from the Red Sea, Gulf of Aden to East Africa came into being [9].

3.1. Stratigraphy

The Termit Basin has experienced two episodes of continental rift deposition in the Early Cretaceous and Paleogene Periods as well as extensive transgression in the Late Cretaceous [12]. The Basin is composed of marine and continental sandstone and mudstone with the max deposition thickness of over 12000 m [12–14]. The sedimentary formations from the old to the young consist of Precambrian basement, Cretaceous, Paleogene, Neogene and Quaternary formations.

3.1.1. Precambrian Basement

Precambrian consists of biotite gneiss, pegmatite, quartz mica schist, phyllite, granite, etc. The minimum age is 568–434 ± 26 Ma which is inferred to be the product of a Pan-African tectonic event [9].

3.1.2. Cretaceous Formation

Lower Cretaceous (K1)

Affected by grabens and half grabens, the Lower Cretaceous has the thickest sediments along boundary faults [15]. Seismic reflections are shown as low-frequency, weak amplitude and discontinuous events. The bottom is in unconformable contact with the basement and the top is in angularly unconformable contact with overlying Upper Cretaceous formations with local truncation [15]. Sedimentary facies include coarse-grain fan delta and subaqueous fan transiting to fine-grain delta and lacustrine facies. Lithologic component consists of alternate layers of sandstone with kiesel, kaolinite and quartz, siltstone and mudstone. The Lower Cretaceous is drilled in Well Donga-1 and Dilia Langrin-1 with a thickness of 246 m and 174 m separately [15].

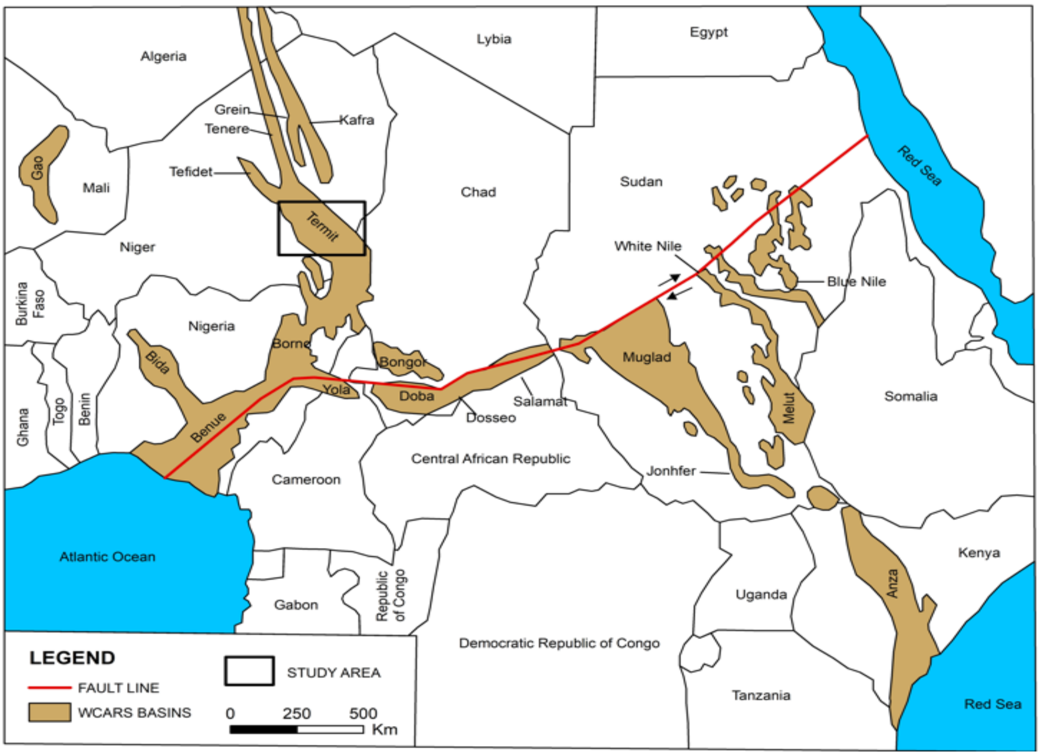

Figure 3. Map showing the WCARS extent, with location of WARS and CARS (modified from[7]).

Upper Cretaceous (K2)

The Upper Cretaceous is composed of marine Donga and Yogou Formation and terrestrial the Madama Formation. In this period, depression dominates the basin with small palaeotopographic variation and stable stratigraphic distribution. Seismic reflections are shown as middle-frequency, strong amplitude and continuous events in Donga and Yogou Formation and as near-blank events in Madama Formation at the top, the former of which are the responses of marine sediments and the latter are the responses of thick terrestrial sandstone [15]. The lower Donga consists of sandstone and gradually transits to mudstone upwards. The bottom section is mainly composed of siliceous, kaolin and some quartzose clean sandstone and some alternate layers of siltstone and a small amount of mudstone [16]. The middle and upper section consists of grey to black mudstone, shale and alternate layers of siltstone and white to light grey finestone. The lower Donga is drilled in the Wells Donga-1 and Dilia Langrin-1 with the thickness of around 1000 m [15]. Yogou Formation is basically composed of argillutite, major source rock in the basin, and some local sandstone at the top. The lithological components include thick grey and dark argillutite sandwiched with grey and dark shale and thin finestone and medium sandstone. The thickness is 500–1000 m. Madama Formation consists of thick sandstone widely spreading in the area and a little of thin argillaceous sandstone (with coal seams) at the top and the bottom. The thickness is 300–700 m [16].

3.1.3. Paleogene Formation

The Paleogene formation consists of lacustrine sediments, which are denuded in local areas of the west platform and north Soudana area. Seismic reflections are shown as alternate responses of middle to high frequency, strong amplitude and continuous events and weak amplitude and discontinuous events with unconformable contacts at the top and the bottom [15]. According to lithologic assemblages, the System could be divided into two sections, i.e. lower Sokor1 and upper Sokor2. Sokor1 Formation mainly contains alternate layers of sandstone and mudstone, which are the sediments of fluvial and delta facies with thickness of 0–800 m. Compared with the Madama Formation, its single sand is inferior in thickness but superior in porosity and permeability [15]. Sokor1 is the major pay zone of the Termit Basin and shows alternate responses of middle to high frequency, strong amplitude and continuous events and weak amplitude and discontinuous events on seismic profiles. Sokor2 Formation is composed of lacustrine mudstone sandwiched with thin sandstone and shows high GR and low resistivity on wireline log. Lithological components include grey and dark mudstone sandwiched with coals with large single thickness and wide distribution. It is a regional cap formation in the area and shows blank reflections on seismic profiles. Deposition thickness is 300–800 m.

3.1.4. Neogene Formation

The Neogene formation is dominated by depression sedimentation and widely distributes in the whole basin with a thickness of 9–500 m. It is basically composed of finestone to coarse-grain sandstone and minerals are mainly quartz and feldspar with a little of clay, which are sediments of fluvial facies [12]. Seismic reflections are shown as middle to low frequency, medium amplitude and medium continuity events. The bottom is in unconformable contact with Paleogene in Soudana. Deposition thickness is 9–500 m.

3.1.5. Quaternary Formatiom

The Quaternary formation is made up of clay, siltstone, finestone and gravel beds. Its surface is covered by desert with a thickness of 10 m (**Figure 4**).

3.2. Structural Units and Structural Styles

The Termit Basin extends in an NW-SE direction on the whole and may be divided into an east belt and a west belt or a south block and a north block with distinct features [15, 16]. There are mainly two groups of faults in NW-SE and NNW-SSE strike separately due to the impacts of superimposed two-stage rifts formed in the Early Cretaceous and Paleogene Period. According to the stage and grade, faults in the basin could be classified into two categories, i.e., sag-controlling faults formed in the Early Cretaceous and succeeded into the Paleogene Period and later faults formed in the Paleogene Period, the former of which basically distributed along the basin boundaries in NW-SE strike and the latter of which would spread along basin boundaries and inside the basin in NW-SE and NNW-SSE strike [17]. Based on the structural model with Paleogene Sokor1 top combined with the discrepancies in tectonic evolutions and tectonic styles, the Termit Basin may be divided into eight structural units as described below (**Figure 5**).

Dinga faulted terrace zone involves a series of NW-SE faults, including early faults formed in the Early Cretaceous and succeeded into the Paleogene Period as well as later faults formed in the Paleogene Period [15, 17]. The former is a series of boundary faults inclined in the NE direction and features steep fractured surface, large vertical throw and large scale and extension (mostly 30–90 km in distance); most of them are basement-involved faults and break through sedimentary formations below Neogene and Quaternary strata [17]. The Faults in Dinga sag are underdeveloped in Early Cretaceous. Some faults in NNW-SSE strike occurred in the Paleogene Period; most of them have small fault throws and short lateral extensions and distributed in the en-echelon pattern. Araga graben consists of three diagonally distributing structural zones, i.e. Dibeilla, Madama and Araga. Compared with those in Dinga faulted terrace, Early Cretaceous sag-controlling faults in this unit are inferior both in quantity and in scale. They may distribute in NW-SE strike with SW inclination and small vertical throw; most of them break through sedimentary formations below Neogene and Quaternary [15, 18]. Later en-echelon faults formed in Paleogene Period extend in NNW-SSE direction in the south and turn to NW-SE direction in the north, nearly parallel to those Early Cretaceous faults. Yogou slope is composed of a series of NW-SE faults. Some of them are NE-inclined faults formed in Early Cretaceous with large throw and extension and succeeded into Paleogene Period with decreased throw. Others are faults developed in Paleogene Period with small throw and short extension [18]. The faults in Trakes slope may also be classified into two groups: one group involves Early Cretaceous faults in NW-SE strike and SW inclination, which are continuous but less active in Paleogene Period; the other group is faults in NNW-SSE strike and NEE inclination, which are formed in Paleogene Period. Both groups in this tectonic unit are of small throws and short extensions [15]. The faults in Moul sag are mainly developed in Paleogene Period in NNW-SSE strike and NEE inclination. These faults distribute in en-echelon pattern with small throw and short extension [15]. Fana low uplift at the Late Cretaceous depositional stage is a low-relief salient in NNW-SSE direction and separates Dinga sag and Moul sag. Faults in this structural unit were mainly formed at Paleogene rifting stage. Similar to Moul sag, faults in Fana are also in NNW-SSE strike and NNE trend [17]. From Fana low uplift northwards to Araga graben and southwards to Yogou slope, Paleogene faults tend to be consistent with Early Cretaceous faults in strike [15]. Soudana uplift lies in the north part of the Termit Basin. Faults formed in Early Cretaceous are in NW-SE strike and NE trend and continue to be active in Paleogene Period with large throw and long extension [15]. Apart from those successive faults from the Early Cretaceous, there are also some anagenetic faults in Paleogene Period with small throw and short extension [18]. Soudana uplift experienced extrusion and uplift at the later stage of Paleogene Period, leading to the denudation of Sokor2 Formation. At two sides of the uplift, Sokor2 Formation is relatively well preserved due to small tectonic uplift and consequent denudation.

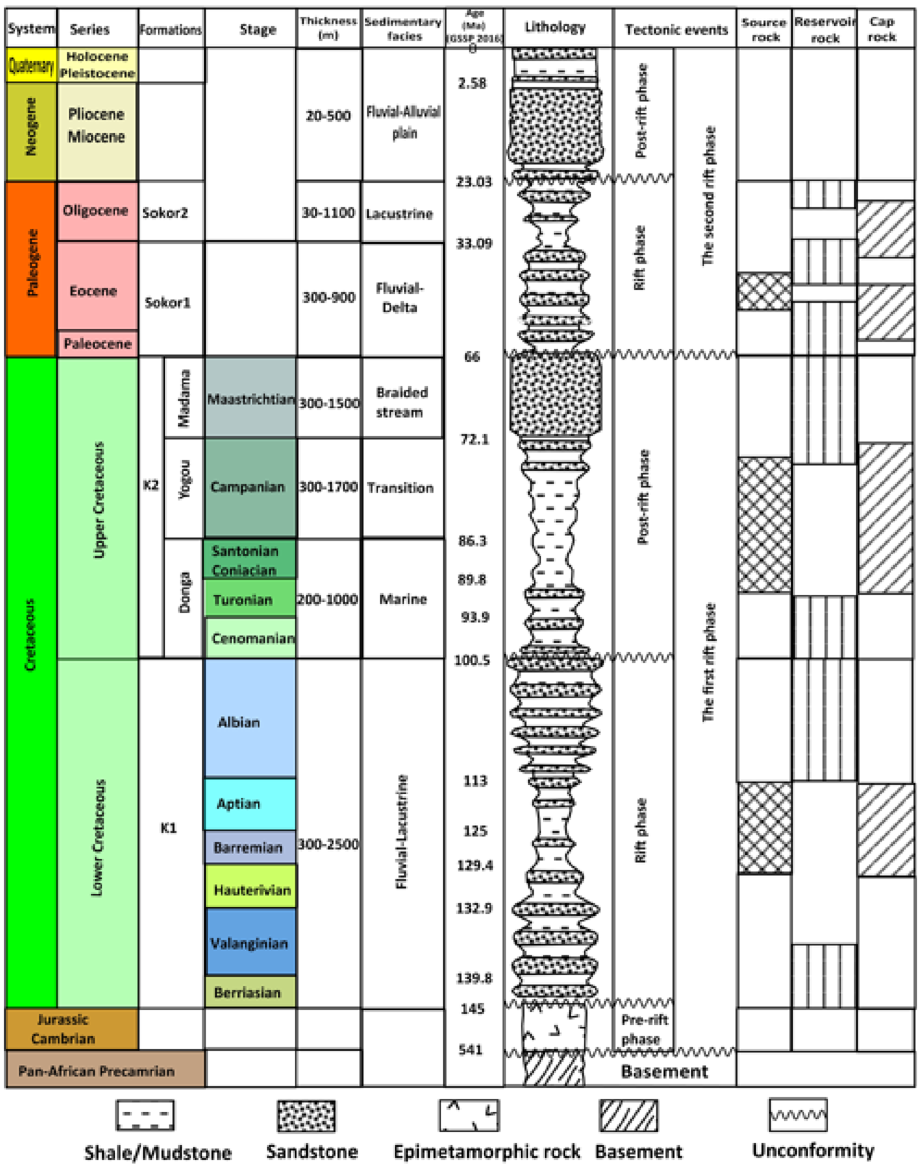

Figure 4. Stratigraphic column of the Termit basin (modified from [7]).

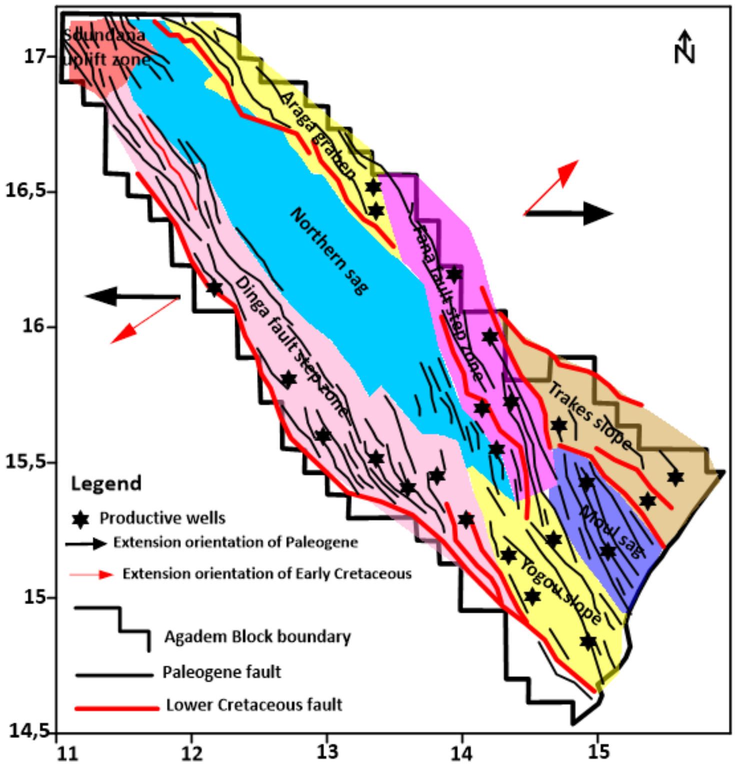

Figure 5. Structural units of the Agadem block (Modified from [15]).

4. Materials and Methods

4.1. Data Used

The data used in this study were acquired by the ARKeX company Ltd. during the period from December 2014 to February 2015. The flight lines (main lines) spacing was 1000 m over the whole block with a direction N137.5°. The tie lines oriented N40° were flown every 5000 m in the main survey area and 3000 m in the southern infill with a direction N20°. Magnetic data are recorded using the Magnetic Recording System DAARC. After verification, these data were subject to corrections. The International Geomagnetic Reference Field (IGRF) was then subtracted from the corrected total field. The values of the residual magnetic field thus obtained were interpolated on a 250 m square grid to obtain the representative map of the residual magnetic field map (RMFM).

In order to obtain maximum information from magnetic data, several filters and transformations were applied to the residual magnetic field map such as the reduction to the north magnetic pole (RTP), the total horizontal derivative (THDR), the tilt angle (TA) and the Euler deconvolution. The THDR and the TA are two methods allowing an edge detection.

4.2. Reduction to the Pole (RTP)

The RTP is a filtering technique that shows the magnetic field transformed to it's equivalent response at the magnetic north pole for vertically magnetized structures. It attempts to simplify the magnetic field by rotating the magnetizing vector to be vertical [19, 20]. The purpose of this transformation is to center anomalies over their causative source by delineating them laterally. This requires knowledge of the direction of magnetization of the magnetic sources [21]. Generally only one declination and inclination value is considered for all the surveyed areas [22]. In the case of this study, 12° for the inclination and 0.9° for the declination were used.

4.3. Total Horizontal Derivative (THDR)

The THDR method has been used since 1982 to locate magnetic boundaries of magnetic structures [23]. According to [24], the THDR method remains a useful and fast way of delineating magnetic boundaries in the subsurface. The THDR maxima are indicative of lateral susceptibility contrasts which are interpreted as geological contacts or structural accidents. Thus, to determine the magnetic lineaments, which correspond to the local maxima, the THDR method has been applied to the RTP map. The THDR is expressed by the following equation:

$$THDR = \sqrt{\left(\frac{\partial M}{\partial x}\right)^2 + \left(\frac{\partial M}{\partial y}\right)^2} \quad (1)$$

Where M is the value of the magnetic field and ∂x, ∂y the first derivatives of the magnetic field M in x and y.

4.4. Tilt Angle (TA)

The TA is one of the conventional local phase filters for enhancing features and causative body edge detection in potential field images. This filter was first developed by [25]. The TA is defined as the ratio of the vertical derivative to the absolute amplitude of the total horizontal derivative :

$$TA = tan^{-1}\frac{\partial M}{\partial z} \Big/ \sqrt{\left(\frac{\partial M}{\partial x}\right)^2 + \left(\frac{\partial M}{\partial y}\right)^2} = tan^{-1}\frac{\partial M}{\partial z}/THDR \quad (2)$$

Where ∂z is the first derivative of the magnetic field M in z.

The TA expression has no dependence on the susceptibility of the underlying bodies. However, all positive TA anomalies relate to positive susceptibility structures which in this case are mainly from magnetic lineaments with widths that can be estimated from their zero contour crossings. But it is important to remember that the zero of the TA is a contour and only part (or parts) of this contour relates to structural edges.

4.5. Euler Deconvolution

The Euler deconvolution calculation is a technique that allows the automatic evaluation of depths. It uses three orthogonal gradients of any potential quantity to estimate the location of a source body and that in theory only pure 2D and 3D sources (e.g. line and point) satisfy this method [26] believe that in practice Euler deconvolution can be applied to fields from causal bodies of arbitrary shapes.

This method allows the location of magnetic contacts at different depths [21]. According to [27], an important consideration in this analysis is the choice of the structural index which describes the rate of magnetic field decay which is related to the shape of the source body. He reports that using the wrong index produces scattered solutions and biased depths. Thus, an index that is too low gives depths that are too low and vice versa. In the case of this study, we chose the value "1" as the structural index (SI) applied to the RTP data.

Following the methodology described by [27], the 3D Euler's homogeneity equation is expressed as:

$$(x - x0)\frac{\partial M}{\partial x} + (y - y0)\frac{\partial M}{\partial y} + (z - z0)\frac{\partial M}{\partial z} = N(B - M) \quad (3)$$

Where x, y and z are the observation coordinates and $x0$, $y0$ and $z0$ are the source coordinates. The constant B is the regional value of the magnetic total field M. Further N is the structural index value for magnetic which depends on the source geometry.

5. Results

5.1. The Residual Magnetic Field Map (RMFM)

The RMFM (**Figure 6**) highlights the effects of the magnetization contrast of the different rock types and the geological structures. This map shows two types of anomalies (circular and ovale) of different sizes and shapes whose intensity ranges from −28,1 nT to 2,82 nT. The circular anomalies can be related to magnetic intrusions. The RMFM shown in general two distinct sectors: the NW and the southern part of the study area show negative anomalies. The SE part of the map is characterized by a dominance of positive anomalies.

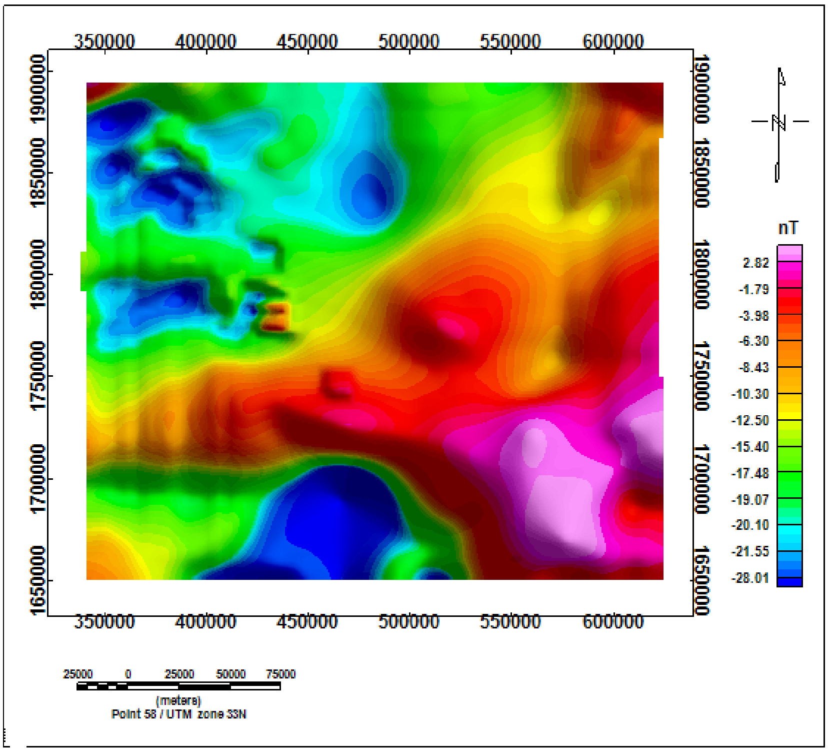

Figure 6. Residual magnetic field map of the studied area.

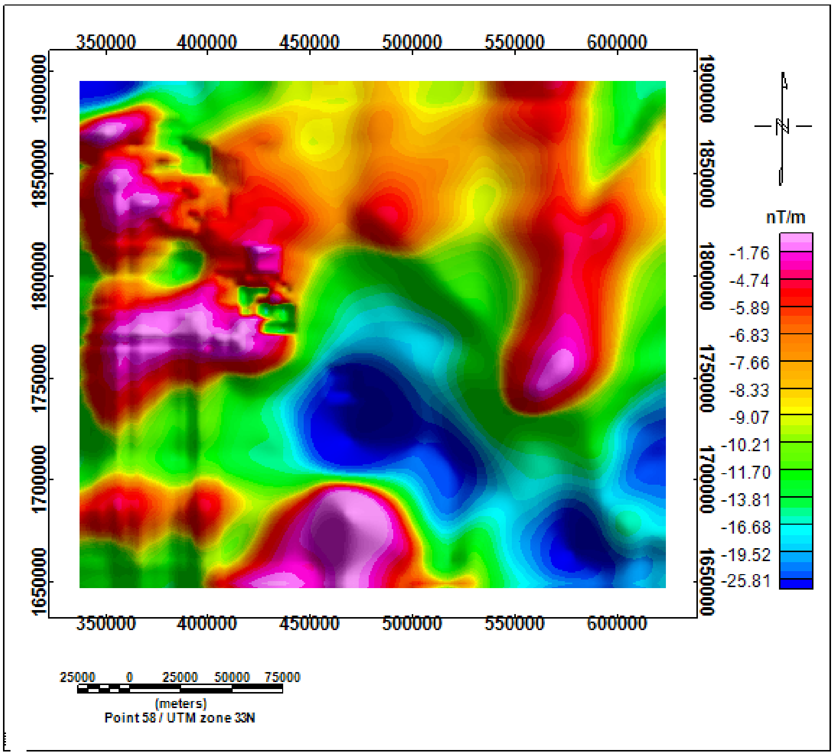

Figure 7. Magnetic anomalies reduced to the pole.

5.2. The RTP Map Analysis

The RTP has been produced in the Fourier domain after an application of a Gaussian low pass filter (1000 m), using a magnetic inclination of 12° and magnetic declination of 0,9 (**Figure 7**).

The lower part of the study area shows negative magnetic anomalies of large amplitudes and long wavelengths, showing NW-SE orientation compatible with the regional deformation trends. This feature indicates a weak magnetization which corresponds to the presence of a strong sedimentary filling.

The rest of the study area is characterized by strong positive magnetic anomalies of large amplitudes and long wavelengths. These anomalies correspond to the alkaline volcanic rocks (nephelinites, basanites, phonolites, trachy-phonolites and quartz-trachytes) whitch took place from Oligocene to Pliestocene volcanic activities [28].

5.3. The THDR Map

The THDR filter was applied to the RTP map to highlight geological contacts and major accidebts. The **Figure 8** shows the different contacts identified from the THDR. We distinguish linear anomalies along the directions: E-W, ENE-WSW, NE-SW, NW-SE,NE-SW and N-S, and circular anomalies which could be inferred to volcanic rocks. These lineaments could be related to the Early Cretaceous and Paleogene rifting phases of the Termit Basin.

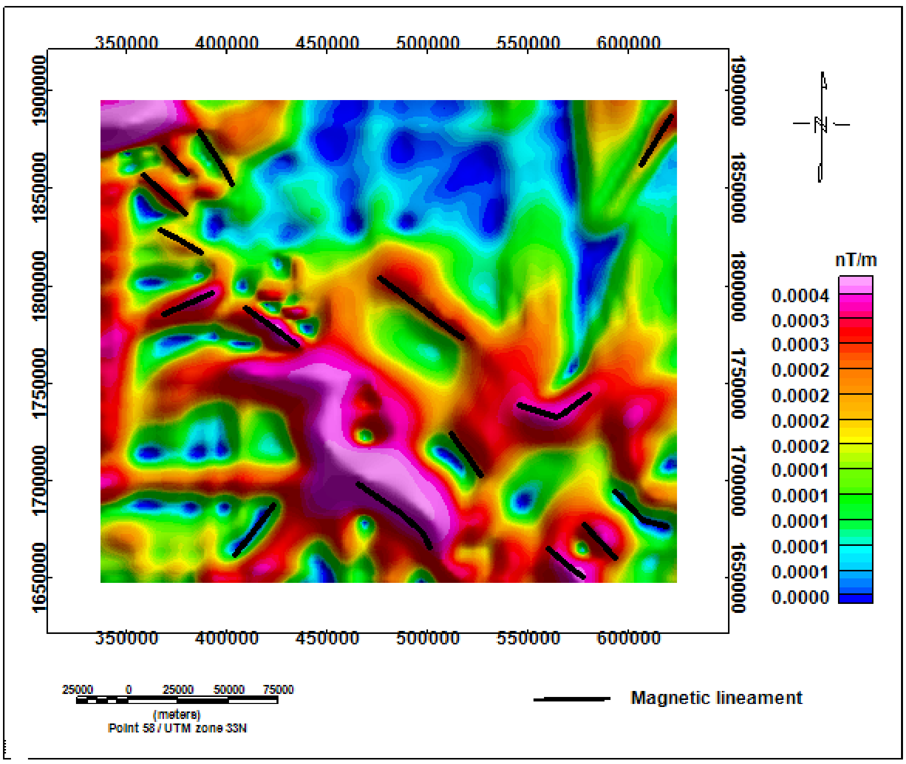

Figure 8. Total Horizontal Derivative map of the studied area.

5.4. The TDR Map

The TDR method allows the location of lateral changes in magnetic susceptibility interpreted as magnetic lineaments. This filter was applied to the reduced magnetic data at the pole, showed results that confirm those obtained by the THDR. Thus it allowed us to detect several lineaments whose orientations are N-S, E-W, WSW-ENE, SW-NE, WNW-ESE, NW-SE and NNW-SSE (**Figure 9**). These lineaments are compatible with the two rifting phases of the Cretaceous and Paleogene that occured in the Termit Basin.

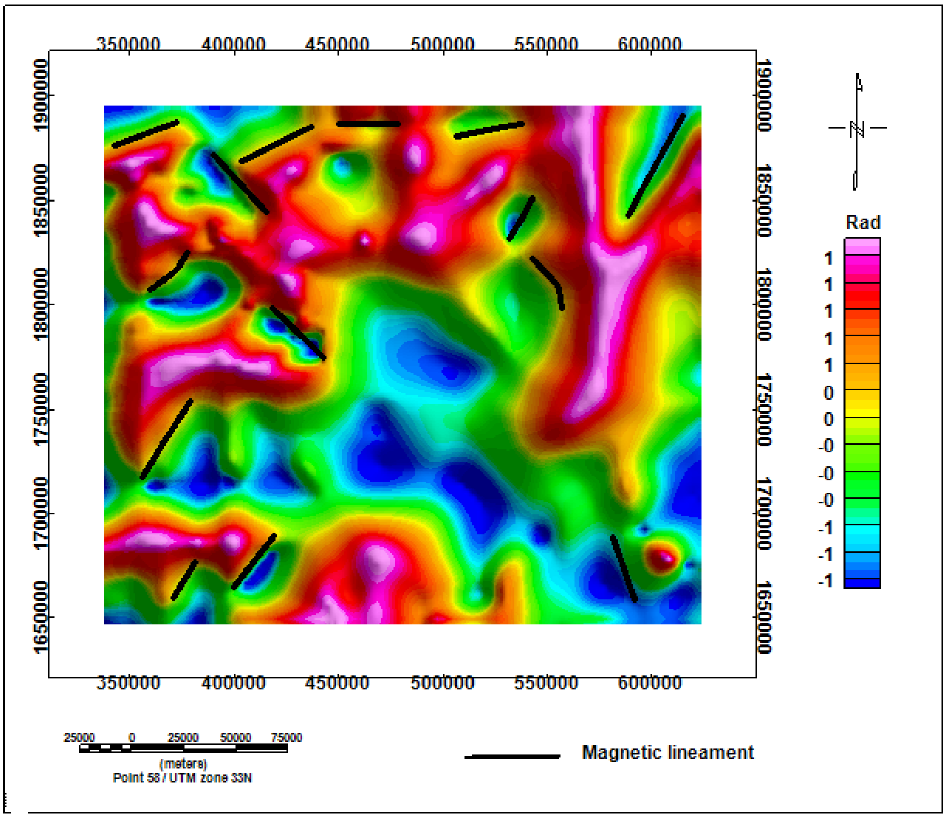

Figure 9. Tilt Derivative map of the study area.

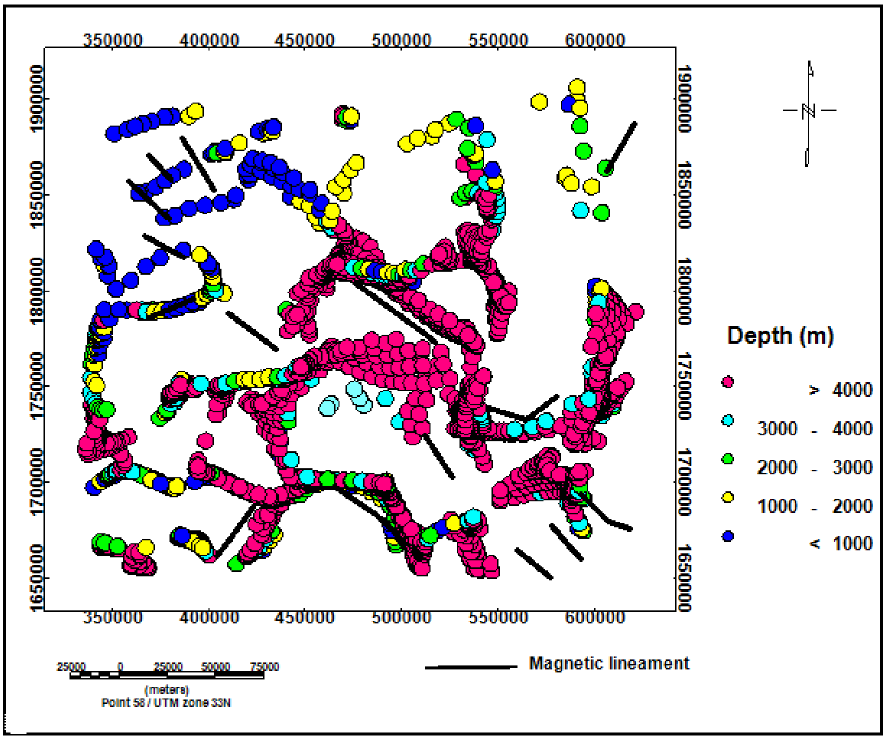

Figure 10. Magnetic source depth estimation map.

5.5. Depth Estimation

In order to locate the magnetized bodies and the fault structures, the Euler Deconvolution was applied to the RTP map of the study area. The first step consisted to determine the horizontal derivatives along x, y and z of the RTP map. Then, the Euler deconvolution was calculated to determine the position and depth of the magnetic sources. However, to obtain a better estimation of the depths, the following parameters have been chosen: structural index (SI) = 1, window size = 10 and error tolerance = 3%.

The obtained Euler solutions are perfectly aligned with the magnetic lineaments of the THDR (**Figure 10**). The depths vary from 1000 m to 4000 m and follow the magnetic lineament trends. The shallow depths are represented by blue dots and the yellow dots indicate the deeper magnetic sources.

The intrusions are responsible for the shallow depth estimates and the deeper estimates are most likely to be related to the basement.

6. Discussions

The interpretation of aeromagnetic data of the Agadem Block, brings new information related to the structural features that characterized the tectonic evolution of the study area. The analysis of the RTP map clearly reflects the hemi-synclinal structure of the Agadem Block in agreement with the overall structure of the Termit basin. In the SE part, the alignment of the negative anomalies of different intensities and different sizes indicates that we are rather in the presence of a synclinorium. The RTP map shows that the study area is asymmetric displaying positive anomalies in the NW part and a pronounced negative anomaly in the SE part indicating a weak magnetization. The overall magnetic anomaly direction reveals NW-SE to NE-SW trending in concordance with the regional tectonic directions. Hence, the short wavelength anomalies can be linked to the Cenozoic volcanic activities. whereas, the long wavelength magnetic anomalies are caused by more deeper sources related to the basement rocks. Moreover, the analysis of THDR, TDR, and Euler deconvolution maps allowed us to highlight the subsurface structure of Agadem block. The analysis of the structural map indicated that the study area is crossed by several new lineaments in different directions : NW-SE, NNW-SSE, E-W, N-S, NE-SW.

7. Conclusions

Airborne magnetism remains an essential tool in the mapping and characterization of deep geological structures such as faults, lineaments and the geometric configuration of sedimentary basins. Thus, through the interpretation of aeromagnetic data, we are able to determine the major geological structures, which affect the study area.

- The analysis of the magnetic anomaly map shows that the Agadem block has areas of low intensity and areas of high magnetic intensity located respectively in the south and the north. The magnetic anomaly map also shows that the anomalies are elongated along the NW-SE direction, corroborating the structural orientation of the study area.
- The volcanic activities whose indices are noted outside the block continued inside during a period prior to the Quaternary cover but spread over normal and reverse periods of the magnetic field prior to those of the Quaternary.
- The analysis of the aeromagnetic data from the reduction to the pole played an important role in the structural study of the Agadem block which shows a folded hemi-syncline structure to the south part. Also, this analysis allowed to highlight sedimentary filling zones with a major petroleum interest.
- Both of the Total Horizontal Derivative and the Tilt Derivative methods highlight magnetic lineaments whose orientations are N-S, E-W, WSW-ENE, SW-NE, WNW-ESE, NW-SE and NNW-SSE.
- In the end, the calculation of the Euler deconvolution, allowed us to determine and locate the magnetic source whose depths vary from 1000 m to 4000 m.

In perspective, we will consider processing medium and long wavelength gravimetric data covering the Agadem block in order to compare the results of aeromagnetism. A synthetic model taking into account the two approaches and the seismic data is quite possible.

Funding

This research received no external funding.

Institutional Review Board Statement

Not applicable.

Informed Consent Statement

Not applicable.

Data Availability Statement

Data will be available on request from the author.

Acknowledgments

This research was carried out as part of the PhD thesis. The authors would like to thank the Ministry of Petroleum of the Republic of Niger for the data made available. Also, we thank reviewers for their helpful comments and recommendation.

Conflicts of Interest

The authors declare no conflict of interest.

References

[1] Dumont, M., Reninger, P.A., Pryet, A., 2018. Agglomerative hierarchical clustering of airborne electromagnetic data for multi-scale geological studies. Journal of Applied Geophysics. 157, 1–9. DOI: https://doi.org/10.1016/j.jappgeo.2018.06.020

[2] Oskooi, B., Maysam, A., 2015. An airborne magnetometry study across Aagros collision zone along Ahvaz-isfahan route in Iran. Journal of Applied Geophysics. 123, 112–122. DOI: https://doi.org/10.1016/j.jappgeo.2015.10.001

[3] Thomas, E., Mougin, B., Debeglia, N., et al., 2002. Apport des levés géophysiques aéroportés à la recherche et à la protection des ressources en eau: application à la région du Léon (Finistère). Office of Geological and Mining Research, Paris, France. p. 63.

[4] Elkhateeb, S.O., Mahmoud, A., Gaballah, A., 2018. Delineation potential gold mineralization zones in a part of central eastern desert, egypt using airborne magnetic and radiometric data. Journal of Astronomy and Geophysics. 7(2), 361–376. DOI: https://doi.org/10.1016/j.nrjag.2018.05.010

[5] Genik, G.J., 1992. Regional framework, structural and petroleum aspects of rift basins in Niger, Chad and the Central African Republic (C.A.R). Tectonophysics. 213, 169–185. DOI: https://doi.org/10.1016/B978-0-444-89912-5.50036-3

[6] Guiraud, R., Maurin, J.C., 1992. Early cretaceous rifts of Western and Central Africa: an overview. Tectonophysics. 213, 153–168. DOI: https://doi.org/10.1016/0040-1951(92)90256-6

[7] Genik, G.J., 1993. Petroleum Geology of Cretaceous-Tertiary Rift Basins in Niger, Chad, and Central African Republic. AAPG Bulletin. 77, 1405–1434. DOI: https://doi.org/10.1306/BDFF8EAC-1718-11D7-8645000102C1865D

[8] Ajakaiye, D.E., Burke, K., 1972. A bouguer gravity map of Nigeria. Tectonophysics. 16(2), 103–115. DOI: https://doi.org/10.1016/0040-1951(73)90134-0

[9] Binks, R.M., Fairhead, J.D., 1992. A plate tectonic setting for Mesozoic rifts of West and Central Africa. Tectonophysics. 213(1–2), 141–151. DOI: https://doi.org/10.1016/0040-1951(92)90255-5

[10] Fairhead, J.D., Binks, R.M., 1991. Differential opening of the central and South Atlantic oceans and the opening of the Central African rift system. Tectonophysics. 187(1–3), 191–203. DOI: https://doi.org/10.1016/0040-1951(91)90419-S

[11] Guiraud, R., William, B., 1997. Senonian basin inversion and rejuvenation of rifting in Africa and Arabia: synthesis and implications to plate-scale. Tectonophysics. 282(1–4), 39–82. DOI: https://doi.org/10.1016/S0040-1951(97)00212-6

[12] Fairhead, J.D., Green, C.M., 1989. Controls on rifting in africa and the regional tectonic model for the nigeria and east Niger rift basins. Journal of African Earth Sciences. 8(2–4), 231–249. DOI: https://doi.org/10.1016/S0899-5362(89)80027-2

[13] Genik, G.J., 1993. Petroleum geology of cretaceous-tertiary rift basins in Niger, Chad and Central African Republic. The American Association of Petroleum Geologists Bulletin. 77(8),

1405–1434. DOI: https://doi.org/10.1306/BDFF8E-AC-1718-11D7-8645000102C1865D

[14] Maurin, J.C., Guiraud, R., 1993. Basement control in the development of the early cretaceous West and Central African Rift System. Tectonophysics. 228, 81–95. DOI: https://doi.org/10.1016/0040-1951(93)90215-6

[15] CNPCNP., 2012. Cretaceous geological study and target evaluation in the Agadem block, Niger. p 218.

[16] Wan, L., Jiguo, L., Fengjun, M., 2014. The petroleum geochemistry of the Termit basin, eastern Niger. Marine and Petroleum Geology. 51, 167–183. DOI: https://doi.org/10.1016/j.marpetgeo.2013.11.006

[17] He, J.S., Jiang, T.L., Peng, F.Z., et al., 2020. Controlling factors of hydrocarbon accumulation in termit rift superimposed basin, Niger. Springer series in Geomechanics and Geoengineering. 44–64. DOI: 10.1007/978-981-15-2485-1_310

[18] CNPCNP., 2013. Cretaceous geological study and target evaluation in the Agadem block, Niger. p 253.

[19] Baranov, V., Nandy, H., 1964. Numerical calculation of the formula of reduction to the magnetic pole. Geophysics. 29(1), 67–79. http://dx.doi.org/10.1190/1.1439334

[20] Macleod, I.N., Jones, K., Dai, T.F., 1993. 3D analytic signal in the interpretation of total magnetic field data at low magnetic latitudes. Exploration Geophysics. 24, 679–687. DOI: https://doi.org/10.1071/EG993679

[21] Grauch, V.J.S., Mark, R.H., Scott, A.M., et al., 2006. Sources of along-strike variation in magnetic anomalies related to intrasedimentary faults: a case study from the Rio Grande Rift, USA. Exploration Geophysics. 37(4), 372–378. DOI: https://doi.org/10.1071/eg06372

[22] Lanza, R., Meloni, A., 2006. The earth's magnetism an introduction for geologists. Springer-Verlag: Berlin/Heidelberg, Germany. p 287.

[23] Cordell, L., 1979. Gravimetric expression of graben faulting in Santa Fe Country and the Espanola Basin, New Mexico: New Mexico Geol. Soc. Guidebook, 30th Field Conf. 59–64. DOI: https://doi.org/10.56577/FFC-30.59

[24] Grauch, V.J.S., Cordell, L., 1987. Limitations of determining density or magnetic boundaries from the horizontal gradient of gravity or pseudogravity data. Geophysics. 52(1), 118–121. DOI: https://doi.org/10.1190/1.1442236

[25] Miller, H.G., Singh, V., 1994. Potential field tilt: a new concept for location of potential field sources. Journal of Applied Geophysics. 32(2–3), 213–217. DOI: https://doi.org/10.1016/0926-9851(94)90022-1

[26] Beiki, M., 2010. Analytic signals of gravity gradient tensor and their application to estimate source location. Geophysics. 75(6), 159–174. DOI: https://doi.org/10.1190/1.3493639

[27] Reid, A.B., Allsop, J.M., Granser, H., 1990. Magnetic interpretation in three dimensions using euler deconvolution. Geophysics. 55(4), 80–91. DOI: https://doi.org/10.1190/1.1442861

[28] Ahmed, Y., Konaté, M., Harouna, M., 2016. Tectonomagmatic reactivation of Téfidet Cretaceous trough during Cenozoic (Aïr, Niger). REV.CAMES. 4(2), 58–66. DOI: https://doi.org/10.2113/GSSGF-BULL.187.2.73